Journal of Power Sources 222 (2013) 112–122

Contents lists available at SciVerse ScienceDirect

Journal of Power Sources

journal homepage: www.elsevier.com/locate/jpowsour

Using electrical analogy to describe mass and charge transport in lithium-ion batteries

S. Raël*, M. Hinaje

Université de Lorraine, GREEN, 2 avenue de la Forêt de Haye, 54516 Vandoeuvre-lès, Nancy, France

HIGHLIGHTS

- We develop a 1D mathematical model of lithium-ion battery.
- We use electrical analogy to solve mass and charge transport equations.
- The model is implemented in a standard software used in electrical engineering.
- The model can be easily employed for the simulation of electrical power systems.

ARTICLE INFO

Article history:
Received 5 June 2012
Received in revised form
20 August 2012
Accepted 22 August 2012
Available online 1 September 2012

Keywords:
Lithium-ion battery
Dynamic modeling
Mass and charge transport
Electrical analogy
Large signal equivalent circuit model

ABSTRACT

This article deals with an electrical model of lithium-ion battery, based on a 1D analog representation of mass and charge transport phenomena. By using an electrical analogy to describe migration and diffusion of species and charges in electrodes and electrolyte, the model can be directly implemented in standard simulation software used in electrical engineering (such as Saber, in our case), so that it can be easily employed for the simulation of electrical systems involving lithium-ion batteries. The paper explains how the analog model is obtained from mass and charge transport equations, then it presents a comparison with results obtained by means of a finite element method. At last, some electrical power systems are simulated in order to show advantages of our modeling method.

1. Introduction

Lithium-ion batteries are based on insertion electrodes, so that their electrical behavior is marked by line effects due to insertion or deinsertion of lithium in electrode active material. As demonstrated in Ref. [1], the slow kinetics of these phenomena limits performances of lithium-ion batteries, particularly in terms of quick charge. It can also lead to unexpected effects, such as plating (metal lithium deposition at electrode surfaces). It is therefore crucial to develop a lithium-ion model that combines a local description of physical phenomena with an implementation suitable for simulation of electrical power systems.

Within a lithium-ion cell take place key processes that are strongly coupled: lithium diffusion in electrode active material, lithium ion migration and diffusion in electrolyte, electron conduction in electrodes, and electrochemical kinetics at electrode/electrolyte interface. Many mathematical models have already been developed in order to describe locally these phenomena, through coupled partial differential equations (PDE) involving space and time. One of the earlier studies, by Doyle et al. [2], led to an isothermal and one-dimensional model, relative to a metal lithium cell. In another significant early work [3], the same authors extended the approach to the modeling of dual lithium ion insertion cell. These works, on which our 1D lithium-ion battery model is based, have been recently improved by Smith and Wang [4] and by Cai and White [5], who introduced thermal heat transfer, temperature dependant parameters and electrothermal coupling. According to results presented in the literature, mathematical lithium-ion battery models are obviously accurate, and enable to study specific local effects. However, they are hardly usable in a system approach, for which a lithium-ion battery model easy to handle is required.

This is the reason why many electrical circuit models have been developed, most often based on the Randles equivalent scheme that represents the electrical behavior of an electrochemical

* Corresponding author. Tel.: +33 383 59 56 54; fax: +33 383 59 56 53.
E-mail address: Stephane.Rael@univ-lorraine.fr (S. Raël).

0378-7753/$ – see front matter © 2012 Elsevier B.V. All rights reserved.
http://dx.doi.org/10.1016/j.jpowsour.2012.08.071

electrode–electrolyte interface. This scheme is generally composed of a series resistance for purely ohmic voltage drops in the electrode and the electrolyte, an electric double layer capacitance in parallel with faradic impedances that describe charges transfer phenomena that occur at the electrode–electrolyte interface, and active material transport in electrode and electrolyte [6,7]. In electrical engineering, this basic Randles equivalent scheme is often reduced to a constant voltage source in series with a constant resistance. Sometimes, like in Ref. [8], a parallel RC dipole is added in series, to describe the electric double layer phenomenon. However, many models improve this basic representation by implementing parameters depending on state of charge (SOC). This is for example the case in Ref. [9], in which a linear variation versus SOC is considered for both open-circuit voltage (OCV) and series resistance. In Ref. [10], battery voltage is computed by a third-order polynomials versus SOC, for different discharge current values. An exponential empirical law is used by Tremblay et al. in Ref. [11], to describe OCV variation versus SOC. The resulting circuit model has been implemented in Refs. [12] and [13], to study power generation systems using lithium-ion storage. This approach has been improved by Tofighi and Kalantar [14], who extended the exponential dependance versus SOC to series resistance and short and long transient parallel RC dipoles. In Ref. [15] at last, Urbain et al. developed an accurate energetical modeling of lithium-ion batteries including SOC and current dependances, electrode porosity and concentration effects, and relaxation. This kind of models can give accurate results, but they are most often empirical, and of course can not describe local effects.

Another way to handle the Randles equivalent scheme is to develop dynamic models based on harmonic response. This approach is used in Refs. [16,17] for modeling lead-acid batteries, in Ref. [18] for modeling NiMH batteries, in Ref. [19] for modeling lithium-ion batteries, and in Ref. [20] for modeling the electrical behavior of a PEM fuel cell. Thus, this approach is widespread in electrochemical device modeling. Nevertheless, although it is most often physics-based, it fundamentally generates only small signal models, which are theoretically not available in large signal conditions, because of non-linearities of electrochemical devices. Moreover, in the case of batteries, it is difficult to obtain an equivalent circuit at a mean current different from zero, because of the SOC dependence of battery behavior. And once again, this kind of models can hardly describe local effects. However, we can find in the literature battery models in Laplace domain that are deduced from a mathematical PDE formulation, such as in Ref. [21]. In this case, local effect description can be associated with system oriented models. This is the purpose of our work, but directly in time domain.

Indeed, we focus in this article on a lithium-ion battery cell electrical model implemented in a simulation software commonly used in electrical engineering to design systems. This model is isothermal and includes transient description, double-layer phenomenon, and 1D mathematical representation of charge and mass transport phenomena in electrodes and electrolyte. For this purpose, we use an electrical analogy of species and charge migration and diffusion equations, so that the model can be directly implemented in a simulation software dedicated to electrical circuit. It can be therefore easily employed for the simulation of electrical systems involving lithium-ion batteries.

In the first part, mass and charge transport equations, electrochemical kinetic equations, and boundary conditions of our lithium-ion battery model are recalled. Then, electrical analogy of mass transport equations in electrodes and electrolyte, and of associated boundary conditions, is detailed, as well as the model assembly. A numerical validation is carried out, by comparing our model results to those obtained by means of a finite element resolution method. Finally, some applications are simulated (series operation, association with a power electronics converter) in order to show advantages of our modeling method.

2. Mathematical 1D model of lithium-ion batteries

A lithium-ion cell is composed of two electrodes, an electrolyte, a porous separator, and two current collectors. We briefly describe hereafter materials commonly used for lithium-ion technology, and principles of operation. Further information can be found in Ref. [22].

Active material of the positive electrode is generally a transition metal oxide containing lithium, mainly cobalt based ($LiCoO_2$). The insertion of lithium operates under a potential ranging between 3.5 V and 4 V (compared to lithium). NMC materials ($LiNi_yMn_zCo_{1-y-z}O_2$) also penetrate the market of portable electronics, because they enable to reduce the content in expensive cobalt. One also uses, in particular for industrial applications, metallic oxides containing nickel ($LiNiO_2$) or iron phosphate ($LiFePO_4$, also called LFP). The insertion material of the negative electrode is a carbon material of coke type, graphite, or amorphous carbon. The insertion of lithium operates under a potential ranging between 0 V and 0.3 V (compared to lithium).

The electrolyte ensures ion migration within the battery. In the case of lithium-ion accumulators, it is a mixture of cyclic and/or linear carbon solvents, such as propylene carbonates (PC), in which a lithium salt, lithium hexafluorophosphate $LiPF_6$ for example, is dissolved. Moreover, the reduction of the electrolyte solvents enables to generate a passivation layer (known as SEI, for Solid Electrolyte Interphase) at negative electrode/electrolyte interface, thus avoiding the degradation of the electrolyte under too low potentials, and protecting carbon material.

The separator constitutes a physical barrier between the two electrodes. Thus, it must be an electronic insulator. It must also be porous, in order to allow the ion migration between electrodes. Separators used in lithium-ion technology usually contain polyethylene (PE) and/or polypropylene (PP).

Lithium-ion accumulators operate according to the "rocking chair" principle [22]: during operation, charge migration within the device is ensured by lithium ions Li^+, which leave the first electrode structure to insert into the second electrode structure. This phenomenon of insertion–deinsertion of lithium ions in electrode materials can be described at the negative electrode by:

$$Li_{y+dy}C_6 \underset{\text{charge}}{\overset{\text{discharge}}{\rightleftharpoons}} Li_yC_6 + dy\cdot Li^+ + dy\cdot e^-, \quad (1)$$

and at the positive electrode by:

$$Li_zMO_2 + dz\cdot Li^+ + dz\cdot e^- \underset{\text{charge}}{\overset{\text{discharge}}{\rightleftharpoons}} Li_{z+dz}MO_2, \quad (2)$$

y ($0 < y < 1$) and z ($0 < z < 1$) being lithium insertion rates in negative and positive electrodes, respectively.

In this section, we first recall assumptions, transport equations and boundary conditions of a mathematical lithium-ion battery model first introduced by M. Doyle, T. F. Fuller and J. Newman in 1993 for a metal lithium cell [2], in 1994 for a dual lithium ion insertion cell [3], and recently improved by Smith and Wang [4]. One will find in Ref. [1] an experimental validation of this mathematical lithium-ion battery model, carried out by K. Smith and C.-Y. Wang on a 6 Ah element. As indicated in Fig. 1, the 1D lithium-ion cell model is composed of three domains:

1) the composite negative electrode, which contains active material particles (Li_yC_6) impregnated with electrolyte,

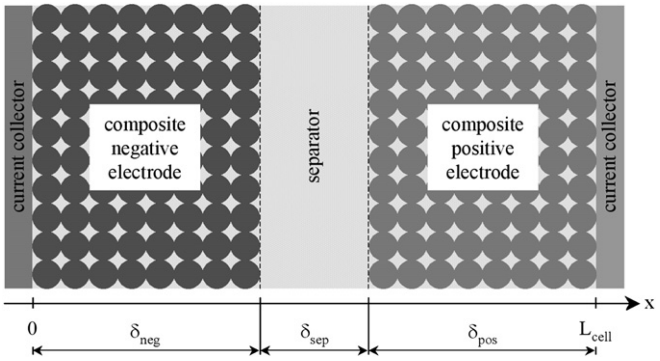

Fig. 1. 1D lithium-ion cell model.

2) the separator, a porous dielectric that ensures electronic insulation and ion migration,
3) the composite positive electrode, which contains active material particles (Li_zMO_2) impregnated with electrolyte.

Assumptions and simplifications adopted in the present model are as follows:

1) the cell temperature remains constant and homogeneous throughout the cell,
2) in the electrolyte phase, mass and charge transports are one-dimensional, along the x direction in Fig. 1. They are both due to diffusion (Fick's diffusion law) and migration (Ohm's law). The convection is neglected,
3) in the solid phase, active material particles, in or out which lithium diffuses, are supposed to be spherical, so that mass transport due to diffusion (Fick's diffusion law) is treated spherical in this phase. Particle radius is considered small enough compared with electrode thicknesses, so that lithium concentration at solid/electrolyte interface is computed as a continuous function of the space variable x. Electron transport through migration (Ohm's law) is one-dimensional, along the x direction in Fig. 1.

The problem has four unknowns: the ionic concentration c_e of the electrolyte, the lithium concentration c_s in active material particles, the electrolyte phase potential ϕ_e, and the solid phase potential ϕ_s. Electrolyte phase unknowns c_e and ϕ_e are available in the three domains, whereas solid phase c_s and ϕ_s are only available in both electrode domains.

2.1. Electrochemical reaction rate

The volume rate G^{Li} of lithium ion generation at the solid/electrolyte interface, i.e. the number of Li^+ moles released in electrolyte phase per time and electrode volume units, is determined by Butler–Volmer kinetics law:

$$G^{Li}(x) = \frac{a_s}{F}\cdot j_0\cdot\left(\exp\left(\alpha_o\frac{\eta(x)}{u_T}\right) - \exp\left(-\alpha_r\frac{\eta(x)}{u_T}\right)\right), \quad (3)$$

where j_0 is the exchange current density, a_s is the electrode active surface per electrode volume unit, η is the local interface overvoltage, u_T is the thermal voltage ($u_T = RT/F$, R being the gas constant, T the temperature, and F the Faraday's constant), α_o and α_r are the oxidation and reduction transfer coefficients, respectively. Active material particles being supposed spherical, and taking into account the active material volume fraction ε_s, the ratio a_s is given by:

$$a_s = \frac{3\cdot\varepsilon_s}{R_s}, \quad (4)$$

R_s being the particle radius, assumed constant in each electrode. At last, we can associate to G^{Li} a volume rate of Li^+ current generation (in A m^{-3}) as follows:

$$j^{Li}(x) = a_s\cdot j_0\cdot\left(\exp\left(\alpha_o\frac{\eta(x)}{u_T}\right) - \exp\left(-\alpha_r\frac{\eta(x)}{u_T}\right)\right). \quad (5)$$

In discharge regime, and contrary to charge regime, j^{Li} is positive at the negative electrode, and negative at the positive electrode.

2.2. Solid phase equations

2.2.1. Lithium transport

Lithium transport in active material particles constituting the solid phase of the electrodes is assumed to be purely diffusive. In a 1D approach, the flux density of lithium in a particle can be written as:

$$\varphi_s(r) = -D_s\cdot\frac{\partial c_s(r)}{\partial r}. \quad (6)$$

A balance of lithium in a particle allows to determine the equation describing the lithium transport in solid phase:

$$\frac{\partial c_s(r)}{\partial t} = \frac{1}{r^2}\,\frac{\partial}{\partial r}\left(D_s\cdot r^2\cdot\frac{\partial c_s(r)}{\partial r}\right). \quad (7)$$

Boundary conditions are of Neumann type. At the particle center, lithium flux density is equal to zero:

$$\varphi_s(0) = 0, \quad (8)$$

and at the solid/electrolyte interface, lithium flux density is linked to electrochemical reaction rate:

$$\varphi_s(R_s) = \frac{j^{Li}(x)}{a_s\cdot F}. \quad (9)$$

2.2.2. Charge transport

In solid phase, charge transport corresponds to electronic conduction. Denoting J_s the associated electronic current density, ϕ_s the potential of the solid phase and $\sigma_{s,eff}$ the effective electronic conductivity of the considered electrode, electron transport in electrodes is described by Ohm's law and can be written in 1D, according to the "x" axis shown in Fig. 1:

$$J_s(x) = -\sigma_{s,eff}\cdot\frac{\partial\phi_s(x)}{\partial x}, \quad (10)$$

the effective electronic conductivity being given, versus the material electronic conductivity σ_s and the active material volume fraction ε_s, by:

$$\sigma_{s,eff} = \varepsilon_s\cdot\sigma_s. \quad (11)$$

A balance of electronic charges in electrode enables to express the charge conservation equation in solid phase as follows, considering that the generation rate of electrons in the solid phase is obviously equal to the generation rate of Li^+ cations in the electrolyte phase:

$$\frac{\partial J_s(x)}{\partial x} = -j^{Li}(x). \quad (12)$$

Boundary conditions at electrode/separator interfaces are characterized by a current density equal to zero, because of the

insulating nature of the separator. What is written, according to the notations defined in Fig. 1:

$$\begin{cases} J_s(\delta_{neg}) = 0 \\ J_s(L_{cell} - \delta_{pos}) = 0 \end{cases}. \quad (13)$$

At electrode/collector interfaces, electronic current density is imposed by the external circuit, which can be written, if I_{cell} is the cell current and A_{cell} the electrode surface:

$$\begin{cases} J_s(0) = I_{cell}/A_{cell} \\ J_s(L) = I_{cell}/A_{cell} \end{cases}. \quad (14)$$

2.3. Electrolyte phase equations

2.3.1. Ion transport

Ion transport in electrolyte phase is a combination of two physical phenomena. The first one is due to the migration caused by local electric field, and the other one is ion diffusion that results from concentration gradients. One demonstrates that species conservation in electrolyte phase leads to the following partial differential equation, involving the ionic concentration c_e, the electrode porosity ε_e, the Li^+ transference number t_p and the effective salt diffusion coefficient in the electrolyte phase $D_{e,eff}$:

$$\varepsilon_e \cdot \frac{\partial c_e(x)}{\partial t} = \frac{\partial}{\partial x}\left(D_{e,eff} \cdot \frac{\partial c_e(x)}{\partial x}\right) + (1 - t_p) \cdot \frac{j^{Li}(x)}{F}. \quad (15)$$

The effective salt diffusion coefficient is given by the Bruggeman relation [23]:

$$D_{e,eff} = \varepsilon_e^p \cdot D_e, \quad (16)$$

where D_e, i.e. the salt diffusion coefficient in the electrolyte phase, is related to anion and cation diffusion coefficients:

$$D_e = \frac{2 \cdot D_{PF_6^-} \cdot D_{Li^+}}{D_{PF_6^-} + D_{Li^+}}. \quad (17)$$

Boundary conditions at electrode/collector interfaces are characterized by a mass flux equal to zero, what can be written as:

$$\begin{cases} \frac{\partial c_e}{\partial x}(0) = 0 \\ \frac{\partial c_e}{\partial x}(L_{cell}) = 0 \end{cases}. \quad (18)$$

At electrode/separator interfaces, the continuity of ionic concentration is applied.

2.3.2. Charge transport

The total ion current density J_e associated with ion transport in the electrolyte phase is the sum of two conduction components (anion and cation transport by migration induced by potential gradient) and two diffusion components (anion and cation transport by diffusion due to concentration gradient). It can be expressed versus the electrolyte concentration c_e and the electrolyte potential ϕ_e as follows:

$$J_e(x) = -\sigma_{e,eff}(x) \cdot \frac{\partial \phi_e(x)}{\partial x} - \sigma_{De,eff}(x) \cdot \frac{\partial \ln(c_e(x))}{\partial x}. \quad (19)$$

The effective ionic conductivity $\sigma_{e,eff}$ of the electrolyte depends on the electrolyte ionic conductivity and the electrode porosity, according to the Bruggeman relation [23]:

$$\sigma_{e,eff} = \varepsilon_e^p \cdot \sigma_e. \quad (20)$$

For the electrolyte ionic conductivity σ_e, which depends on the electrolyte concentration, we will make use of the following empirical law [4]:

$$\sigma_e(x) = 0.00158 \cdot c_e(x) \cdot \exp\left(-5.363 \times 10^{-5} \cdot c_e^{1.4}(x)\right). \quad (21)$$

If the electrolyte potential ϕ_e is refered by a lithium reference electrode at the average electrolyte concentration (corresponding to the OCV measurement conditions), the effective diffusional ionic conductivity $\sigma_{De,eff}$ of the electrolyte is given by:

$$\sigma_{De,eff} = 2 \cdot u_T \cdot (t_p - 1) \cdot \sigma_{e,eff}. \quad (22)$$

Lastly, the balance of ionic charges enables to express the charge conservation equation in electrolyte phase as follows:

$$\frac{\partial J_e(x)}{\partial x} = j^{Li}(x). \quad (23)$$

It can be noticed that the cell current density J_{cell}, equal to the sum of electron current density J_s in solid phase and ion current density J_e in electrolyte phase, has a divergence equal to 0 (Eqs. (12) and (23)), and therefore is constant throughout the cell.

Electrode/collector interfaces are characterized by a purely electronic current density, so that ion current density is equal to zero at these bondaries. Considering Eq. (18), this can be simplified in:

$$\begin{cases} \frac{\partial \phi_e}{\partial x}(0) = 0 \\ \frac{\partial \phi_e}{\partial x}(L_{cell}) = 0 \end{cases}. \quad (24)$$

At electrode/separator interfaces, the continuity of ion current density is applied.

2.4. OCV, electrode overvoltages and cell voltage

Electrode equilibrium potentials are local variables that depend on lithium insertion rate at the surface of solid phase particles, i.e. on the ratio $c_{s,e}(x)/c_{smax}$ between lithium concentration at $r = R_s$ and maximum lithium concentration in solid phase. Curves plotted hereafter in Fig. 2 have been determined by means of empirical formula given in Ref. [4]. For implementing the model in Comsol Multiphysics or in Saber, we will make use of tables associated with these curves.

The local electrode overvoltage involved in the expression of the electrochemical reaction rate j^{Li} (Eq. (5)) is equal to the difference between the interfacial voltage and interfacial equilibrium voltage. It is therefore expressed as a function of the potential of the solid phase ϕ_s, the potential of the electrolyte phase ϕ_e, and the electrode equilibrium potential U as follows:

$$\eta(x) = (\phi_s(x) - \phi_e(x)) - U(x). \quad (25)$$

Once again, it should be noticed here that in this formulation commonly used in the literature, the electrolyte potential ϕ_e is referred by a lithium reference electrode at the average electrolyte concentration, corresponding to the OCV measurement conditions. As a result, the electrode equilibrium voltage U involved in Eq. (25) only depends on the local insertion rate $c_{s,e}(x)/c_{smax}$, the theoretical effect of the local electrolyte concentration on electrochemical kinetics being included in the expression the effective diffusional ionic conductivity $\sigma_{De,eff}$.

Finally, the cell voltage, which is the potential difference between the two current collectors, is therefore equal to the difference of solid phase potentials at $x = L_{cell}$ and $x = 0$:

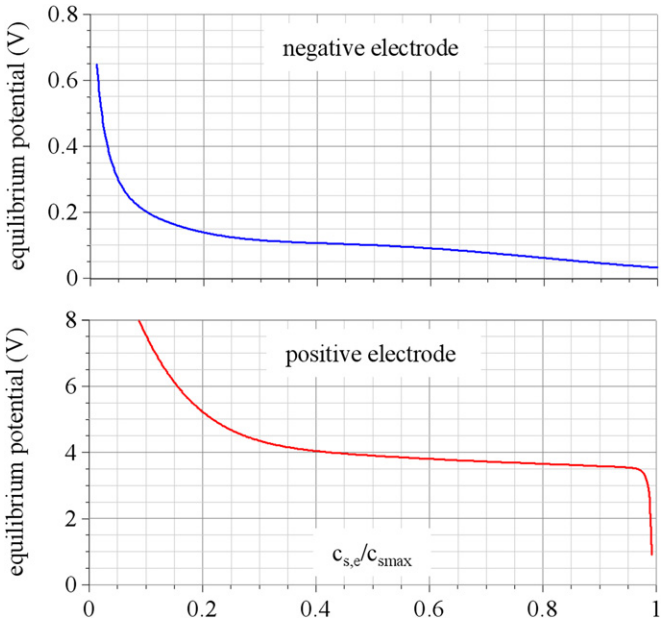

Fig. 2. Electrode equilibrium potentials versus lithium insertion rate.

$$V_{\text{cell}} = \phi_s(L_{\text{cell}}) - \phi_s(0). \tag{26}$$

3. Lithium-ion battery modeling using electrical analogy

3.1. Modeling lithium transport in solid phase

Space discretization of Eqs. (6) and (7) leads to the following system, for the description of lithium diffusion in active material particles constituting the solid phase:

$$\begin{cases} c_s(r+\Delta r) = c_s(r) - \dfrac{\Delta r}{4\pi r^2 \cdot D_s} \cdot N_s(r) \\ N_s(r+\Delta r) = N_s(r) - \left(\dfrac{4}{3}\pi\left((r+\Delta r)^3 - r^3\right)\right) \cdot \dfrac{dc_s}{dt} \end{cases}, \tag{27}$$

Δr being the space discretization step, and N_s being the lithium molar flow within active material particles, defined in spherical coordinates versus the lithium molar flow density φ_s as follows:

$$N_s(r) = 4\pi r^2 \cdot \varphi_s(r). \tag{28}$$

This non-linear system can be computed using an electrical analogy, for which lithium concentration and molar flow are assimilated to voltage and current, respectively. Fig. 3 presents the equivalent electrical scheme of lithium diffusion in a spherical particle element. For more accuracy and for convenience regarding boundary conditions, a two-order circuit is implemented, with the following component expressions:

$$\begin{cases} R_{Li1} = \dfrac{\Delta r/2}{4\pi(r+\Delta r/2)^2 \cdot D_s} \\ R_{Li2} = \dfrac{\Delta r/2}{4\pi(r+\Delta r)^2 \cdot D_s} \\ C_{Li1} = \dfrac{4}{3}\pi \cdot \left((r+\Delta r/2)^3 - r^3\right) \\ C_{Li2} = \dfrac{4}{3}\pi \cdot \left((r+\Delta r)^3 - (r+\Delta r/2)^3\right) \end{cases}. \tag{29}$$

Lithium diffusion in solid phase is then described by associating in series such equivalent circuits. In the analogical model presented here, a space discretization in 10 elements is used for each electrode ($\Delta r = R_s/10$). Fig. 4 depicts input, output and boundary conditions of the resulting lithium diffusion model. Model input, i.e. electrochemical reaction rate j^{Li}, is required for setting boundary molar flow conditions, according to Eq. (9) that becomes here:

$$N_s(R_s, x) = 4\pi R_s^2 \cdot \frac{j^{Li}(x)}{a_s \cdot F}. \tag{30}$$

Model output, the lithium insertion rate at the surface of active material particles, enables the calculation of the local electrode equilibrium potential. Boundary conditions, i.e. Eqs. (8) and (30) for lithium molar flows at $r = 0$ and $r = R_s$, are described by means of an open circuit and a current source, respectively.

3.2. Modeling charge transports and mass transport in electrolyte phase

Electronic and ionic currents being denoted I_s ($I_s = A_{\text{cell}} J_s$) and I_e ($I_e = A_{\text{cell}} J_e$), respectively, space discretization of Eqs. ((10), (12), (15), (19) and (23) leads to:

$$\begin{cases} \begin{cases} \phi_s(x+\Delta x) = \phi_s(x) - R_{s,\text{elt}} \cdot I_s(x) \\ I_s(x+\Delta x) = I_s(x) - I_{\text{elt}}(x) \end{cases} \\ \begin{cases} c_e(x+\Delta x) = c_e(x) - R_{\text{ion}} \cdot N_e(x) \\ N_e(x+\Delta x) = N_e(x) + N_{\text{ion}}(x) - C_{\text{ion}} \cdot \dfrac{dc_e(x)}{dt} \end{cases} \\ \begin{cases} \phi_e(x+\Delta x) = \phi_e(x) - R_{e,\text{elt}} \cdot I_e(x) - V_{\text{elt}}(x) \\ I_e(x+\Delta x) = I_e(x) + I_{\text{elt}}(x) \end{cases} \end{cases}, \tag{31}$$

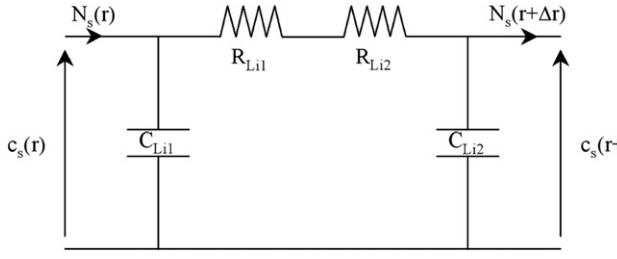

Fig. 3. Equivalent circuit of lithium diffusion in an element of solid particle.

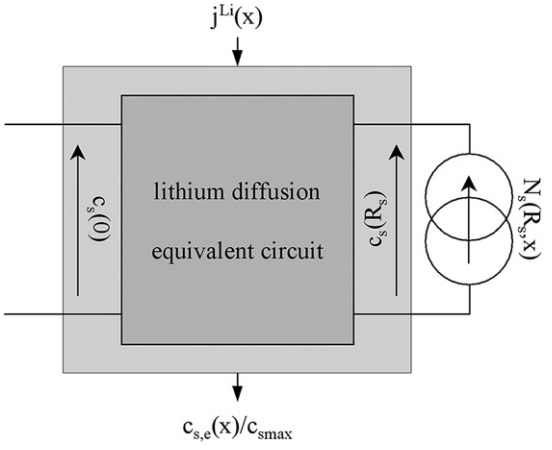

Fig. 4. Electrical analogy of lithium diffusion in electrode solid phase particles.

with the following expressions for charge transport parameters:

$$\begin{cases} R_{s,elt} = \dfrac{\Delta x}{A_{cell}\cdot\sigma_{s,eff}} \\ R_{e,elt} = \dfrac{\Delta x}{A_{cell}\cdot\sigma_{e,eff}} \\ I_{elt}(x) = A_{cell}\cdot\Delta x\cdot j^{Li}(x) \\ V_{elt}(x) = 2u_T\cdot(t_p-1)\cdot\dfrac{c_e(x+\Delta x)-c_e(x)}{c_e(x)} \end{cases}, \quad (32)$$

and the following parameters for mass transport in the electrolyte phase:

$$\begin{cases} R_{ion} = \dfrac{\Delta x}{A_{cell}\cdot D_{e,eff}} \\ C_{ion} = \varepsilon_e\cdot A_{cell}\cdot\Delta x \\ N_{ion}(x) = A_{cell}\cdot\Delta x\cdot(1-t_p)\cdot\dfrac{j^{Li}(x)}{F} \end{cases}, \quad (33)$$

Δx being the space discretization step. This equation system, available in both electrodes, can be computed using the equivalent electrical scheme depicted in Fig. 5. In separator, solid phase equations of Eq. (31) and associated equivalent scheme are of course not to be considered.

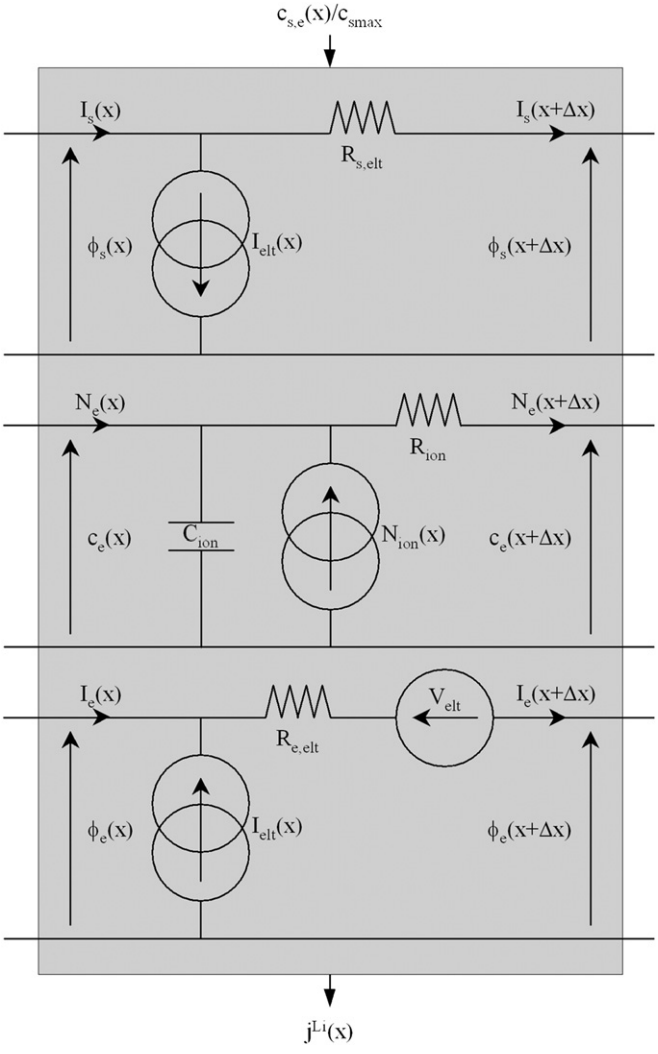

Fig. 5. Equivalent circuit of charge and mass transports in an element of cell (electrode or separator).

The lithium insertion rate $c_{s,e}(x)/c_{smax}$ at the surface of active material particles, determined by the model of lithium diffusion in solid phase, enters the cartesian model for calculating the local electrode equilibrium potential (by means of look-up tables associated with curves of Fig. 2). Then, the local electrode overvoltage η and the electrochemical reaction rate j^{Li} are evaluated according to Eq. (25) and to Eq. (5), respectively. This last variable is required to compute current creation terms (I_{elt} of Eq. (32) and N_{ion} of Eq. (33)), and is also used as an input of the solid phase diffusion model.

Charge transport in solid phase, and mass and charge transports in electrolyte phase, are described by associating in series such equivalent circuits. In our analogical model, a space discretization in 10 elements is used for each electrode ($\Delta x = \delta_{neg}/10$ or ($\Delta x = \delta_{pos}/10$), and for separator ($\Delta x = \delta_{sep}/10$).

3.3. Lithium-ion battery model implementation

Fig. 6 presents the complete lithium-ion battery model that has been implemented in Saber software. It combines:

1) analogical transport models previously described, which calculate concentrations c_e and c_s, electrical potentials ϕ_e and ϕ_s, mass flows N_e and N_s, electrical currents I_e and I_s, overvoltage η and electrochemical reaction rate j^{Li},
2) a controlled voltage source, which couples the electrical model to the transport model via the voltage across the cell.

As depicted in Fig. 6, boundary conditions on electronic current I_s at electrode/separator interfaces (Eq. (13)), and on c_e and I_e at electrode/collector interfaces current (Eqs. (18) and (24)) are treated by means of floating points (corresponding circuits are opened at these interfaces). Boundary conditions on I_s at electrode/collector interfaces (Eq. (14)) are implemented by current sources, equal to I_{cell}. At last, continuity conditions for c_e and I_e at electrode/separator interfaces are naturally modeled by connecting corresponding electrode and separator circuits.

To compute the transport model, a potential reference and initial conditions on concentrations are needed. The potential reference is set at the negative terminal (i.e. $\phi_s(0) = 0$). Initial electrolyte concentration is chosen constant throughout the whole electrolyte domain, and equal to the average electrolyte concentration $c_{e,mean}$. Initial lithium concentrations in solid phases are also chosen constant throughout considered domains, and equal to:

$$c_{s,init} = c_{s,0} + \frac{SOC_{init}}{100}\cdot(c_{s,100} - c_{s,0}), \quad (34)$$

where SOC_{init} is the initial state of charge (in %), and $c_{s,0}$ and $c_{s,100}$ are the lithium concentrations in solid phase when the cell is fully discharged or charged, respectively.

4. Comparison with the model solved by finite element method

The 1D mathematical model of lithium-ion battery described in section 2 has also been implemented in commercial software that enables multiphysics modeling (Comsol Multiphysics, in our case). The resolution is based on the finite element method, each domain is discretized in 40 elements. The aim of this section is to compare results given by this finite element multiphysics software, to those obtained by means of a analogical representation of transport phenamena implemented in Saber software.

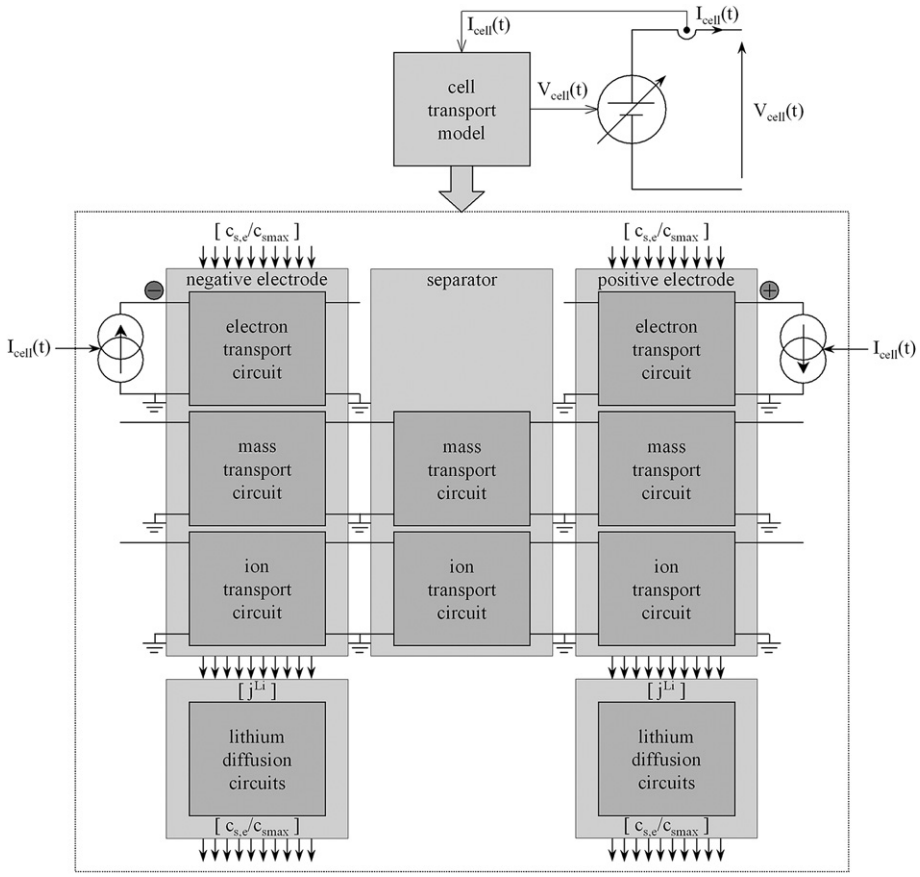

Fig. 6. Lithium-ion cell model.

Table 1
Model parameters [4].

Parameter	Negative electrode	Separator	Positive electrode
Thickness δ [μm]	50	25.4	36.4
Particle radius R_s [μm]	1	–	1
Solide phase volume fraction solide ε_s [−]	0.580	–	0.500
Electrolyte phase volume fraction ε_e [−]	0.332	0.500	0.330
Cell area A_{cell} [m^2]	1.0452	1.0452	1.0452
Max solid phase conc. c_{smax} [mol dm^{-3}]	16.1	–	23.9
Insertion rate $c_{s,e}/c_{smax}$ at SOC = 0% [−]	0.216	–	0.936
Insertion rate $c_{s,e}/c_{smax}$ at SOC = 100% [−]	0.676	–	0.442
Average electrolyte conc. $c_{e,mean}$ [mol dm^{-3}]	1.2	1.2	1.2
Exchange current density j_0 [A m^2]	36	–	26
Oxydation transfer coefficient α_a [−]	0.5	–	0.5
Reduction transfer coefficient α_r [−]	0.5	–	0.5
Solid phase Li diffusion coef. D_s [m^2 s^{-1}]	2×10^{-16}	–	3.7×10^{-16}
Electronic conductivity σ_s [S m^{-1}]	100	–	10
Electrolyte phase diffusion coef. D_e [$m^2.s^{-1}$]	2.6×10^{-10}	2.6×10^{-10}	2.6×10^{-10}
Electrolyte ionic conductivity σ_e [S m^{-1}]	Eq. (21)	Eq. (21)	Eq. (21)
Bruggeman exponent p [−]	1.5	1.5	1.5
Li^+ transference number t_p [−]	0.363	0.363	0.363

Table 1 hereafter details geometric, concentration and physical parameters required for model simulation. These figures come from the reference [4]. Notice that the cell capacity is 6 Ah.

4.1. Simulating discharges at constant current

Fig. 7 presents cell voltage and insertion rate curves obtained, when simulating a complete discharge at 6 A (C rate), from a fully charged state (SOC=100%). Insertion rates are evaluated on the surface of active material particles ($r = R_s$), at electrode/collector interfaces ($x = 0$ and $x = L_{cell}$). Curves in black are associated with the finite element method, and curves in grey with our model using electrical analogy. It can be clearly observed that the two models nearly give the same results. A really little difference appears on cell voltages at the end of discharge, mainly due to the sharp variation of positive electrode OCV when insertion rate $c_{s,e}/c_{smax}$ is within the interval [0.98, 1]. For example, after 1 h discharge, the finite element method gives 3.375 V for cell voltage, 0.176 and 0.959 for insertions rates. Corresponding figures obtained by electrical analogy method are 3.376 V, 0.177 and 0.959, respectively. Other example, a cell voltage of 3 V is obtained at $t = 3774$ s with the finite element method, and at $t = 3778$ s with our analogy method. Associated insertion rates are nearly identical. It can be concluded that the two resolution methods gives same results for slow regimes.

Fig. 8 presents the same kind of comparison as previously, but for a 60 A (10C rate) complete discharge. Once again, it can be observed a really fine agreement between the two resolution methods, and a little difference on cell voltages at the end of discharge (a cell voltage of 2.7 V is obtained at $t = 232$ s with the finite element method, and at $t = 234$ s with our analogy method).

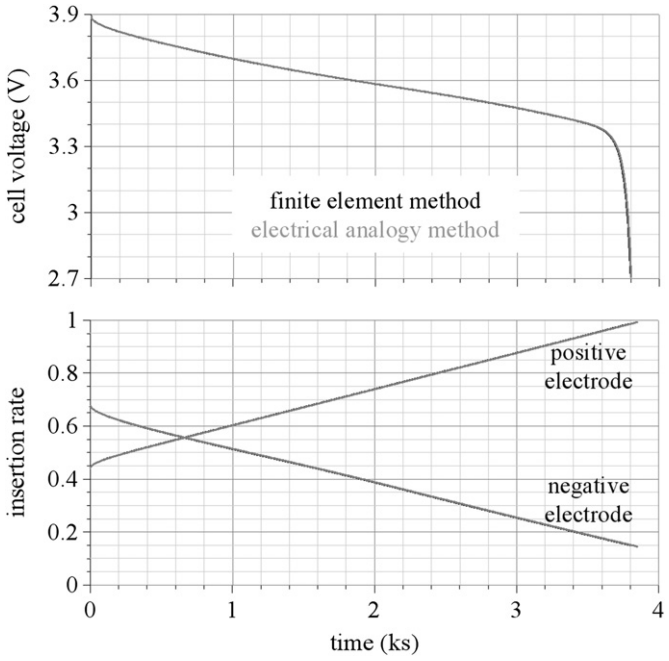

Fig. 7. Simulation of a C complete discharge: cell voltage and insertion rates $c_{s,e}/c_{smax}$ at electrode/collector interfaces (initial SOC: 100%, temperature: 300 K).

4.2. Simulating transient regimes and relaxation

Fig. 9 presents simulated voltage responses to a charge or discharge current step The initial current is zero, the step amplitude is 120 A, the initial SOC is 43% (corresponding to an OCV of 3.6 V), and the temperature is 300 K. It can be observed a really little difference during the first 500 ms. Further simulations have shown that it was mainly due to discretization. Indeed, results became nearly identical if each domain of the finite element model is discretized in 10 elements, as for our model, instead of 40 elements.

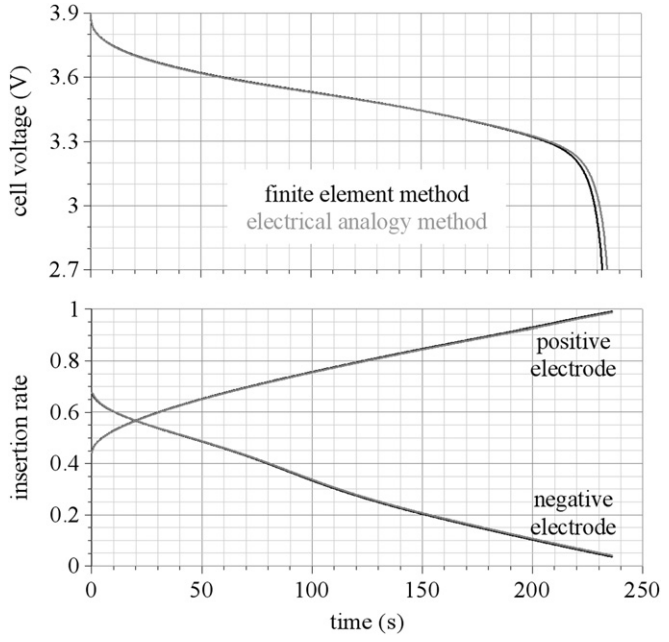

Fig. 8. Simulation of a 10C complete discharge: cell voltage and insertion rates $c_{s,e}/c_{smax}$ at electrode/collector interfaces (initial SOC: 100%, temperature: 300 K).

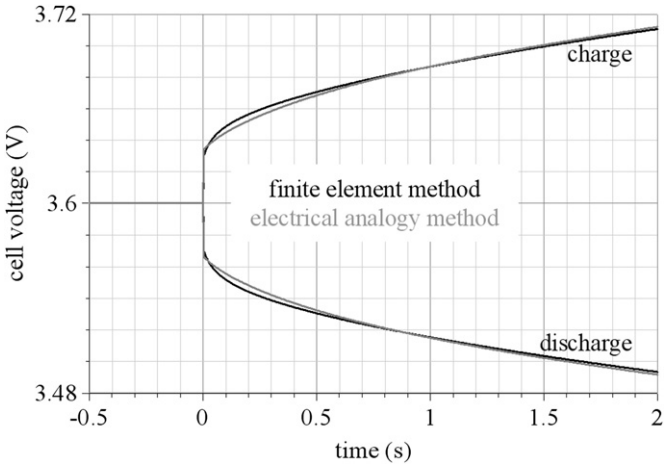

Fig. 9. Simulated responses to a 20C charge or discharge current step (initial current: 0 A, initial SOC: 43% (OCV = 3.6 V), temperature: 300 K).

Last, Fig. 10 shows relaxation curves, following a charge or discharge regime at 60 A (10C rate) during 180 s, the initial SOC being 0% or 100%, respectively. Once again, the comparison between the two models demonstrates really good agreement.

4.3. Advantages of the electrical analogy method

Compared with the finite element method, our electrical analogy modeling method enables direct implementation of the model in standard simulation software used in electrical engineering. Consequently, it can be easily employed for the simulation electrical systems using lithium-ion batteries, as illustrated in section 5. One can also take advantages of the usual environment of electrical engineering simulation software to perform specific analyses, such as parametric studies, impedance spectroscopy, investigation on charge or discharge strategies.

Even in terms of phenomenon modeling, our electrical analogy method can provide facilities. For example, modeling the electric double layer (EDL) phenomenon through a distributed capacitive coupling between solid and electrolyte phases, in a circuit software environment, is quite obvious. In our case, we only need to add a capacitance $C_{DL,elt}$ between the two circuits describing electronic and ionic charge transport in electrodes (cf. Fig. 5), with:

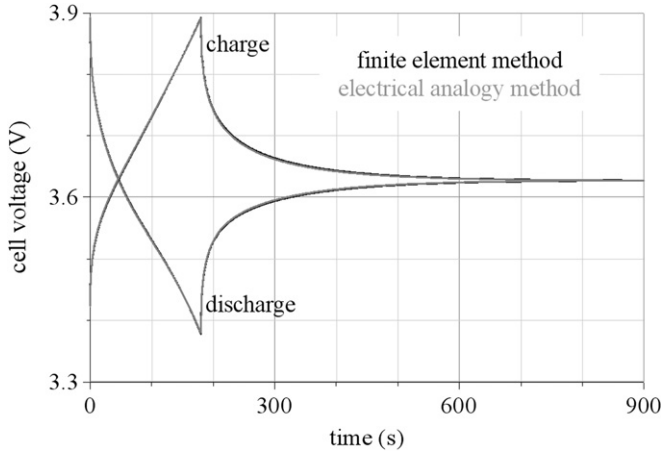

Fig. 10. Simulated cell voltage relaxation, following a 10C/180 s charge or discharge (initial SOC before charge: 0%, initial SOC before discharge: 100%, temperature: 300 K).

$$C_{DL,elt} = \frac{\Delta x}{\delta} \cdot C_{DL}, \tag{35}$$

C_{DL} being the EDL capacitance of the electrode. For illustration, Fig. 11 compares the simulated voltage responses to a 20C charge or discharge current step, as depicted in Fig. 9, with the same kind of simulation carried out with description of electric double layer effect. For this purpose, electrode EDL capacitances are defined versus the cell EDL capacitance $C_{DL,cell}$ as follows:

$$\begin{cases} C_{DL,neg} = \left(1 + \dfrac{\delta_{neg}}{\delta_{pos}}\right) \cdot C_{DL,cell} \\ C_{DL,pos} = \left(1 + \dfrac{\delta_{pos}}{\delta_{neg}}\right) \cdot C_{DL,cell} \end{cases}. \tag{36}$$

Another example is the modeling of the solid/electrolyte interface (SEI) layer, by an additional specific resistance R_{SEI} (in $\Omega\ m^2$) which modifies the volume rate Li^+ current generation, as proposed by Smith and Wang [1,4]:

$$\begin{cases} j^{Li}(x) = a_s \cdot j_0 \cdot \left(\exp\left(\alpha_o \dfrac{\nu(x)}{u_T}\right) - \exp\left(-\alpha_r \dfrac{\nu(x)}{u_T}\right)\right) \\ \nu(x) = \eta(x) - \dfrac{R_{SEI}}{a_s} \cdot j^{Li}(x) \end{cases}. \tag{37}$$

This kind of circular definition is not allowed by the multiphysics finite element software we use, whereas it does not present any problem of resolution with our electrical engineering simulation software, which of course includes a Newton iteration algorithm.

5. Application on electrical power systems

In this section, we give two examples of use of our lithium-ion battery model for simulation of electrical systems. The first aims to show how our model can help battery conception (cell balancing, battery management system). It deals with series association of lithium-ion cells. Implementing such a battery is really easy and natural, when using an electrical circuit simulation software. Indeed, the single cell model previously described, which appears like a two-port component (in our case, a current-controlled voltage source, as depicted in Fig. 6), can be added to the software library, with a symbol and a list of parameters. Then, it can be used in an electrical sketch like any other component of the library.

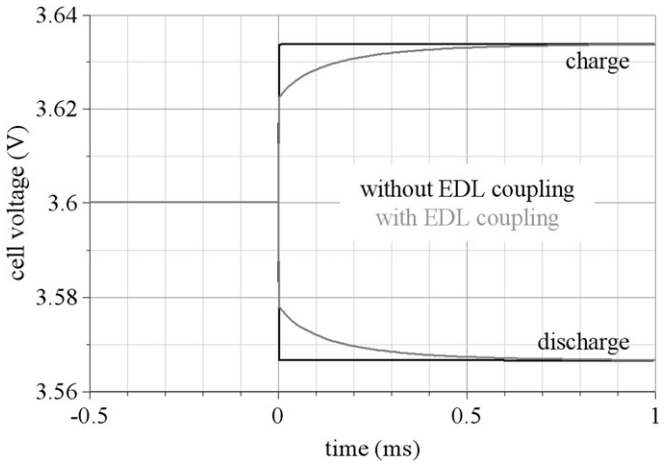

Fig. 11. Simulated responses to a 20C charge or discharge current step (initial current: 0 A, initial SOC: 43% (OCV = 3.6 V), cell EDL capacitance : 10 F, temperature: 300 K).

In particular, it can be associated in series with other single cells, with possible different parameter values. This is what is simulated hereafter.

Fig. 12 presents cell voltages, battery voltage and insertion rate curves obtained, when simulating a complete charge of a lithium-ion battery at 60 A (10C rate). The battery consists of five elements in series, with identical initial SOC. Solid phase diffusion coefficients of cell 1 is assumed to be twice lower than those of other cells, because of a different temperature for example. Insertion rates are evaluated on the surface of active material particles ($r = R_s$), at the electrode/separator interfaces ($x = \delta_{neg}$ and $x = L_{cell} - \delta_{pos}$), which are the most critical places for insertion rate, as far as solid phase conductivities (100 S m^{-1} at the negative electrode, and 10 S m^{-1} at the positive electrode) are much greater than electrolyte ionic conductivity (about 0.6 S m^{-1}). As lithium diffusion in solid phase of cell 1 is slower than in other cells, lithium concentration near particle surface of cell 1 is greater, so that the voltage of this cell increases faster than the others. As a result, cell 1 voltage quickly reaches its rated value (about 4 V), long before the battery rated voltage (about 20 V) is obtained. Moreover, in the simulation carried out here, a plating phenomenon (metal lithium deposition at negative electrode) can be for seen. Through this quite simple example, it is clear that cell balancing is necessary.

The second application, which consists of instantaneous modeling of a power electronic converter involving a lithium-ion battery, aims to demonstrate that our model is suitable for electrical system simulation. In the case presented here, as depicted in Fig. 13, the converter is a current regulated two-quadrant chopper, linking a lithium-ion battery constituted with 14 elements in series (all elements are assumed identical), and a DC link (voltage: 240 V). The input inductance value is 1 mH, and switching frequency is 2 kHz. Battery current regulation is achieved by means of a PI corrector, in association with a PWM generator. Fig. 14 hereafter shows battery current and voltage waveforms, in response of changes in current reference (0 A over [0 s, 5 s], −60 A over [5 s, 15 s], 0 A over [15 s, 20 s], 60 A over [20 s, 30 s], and 0 A over [30 s, 35 s]).

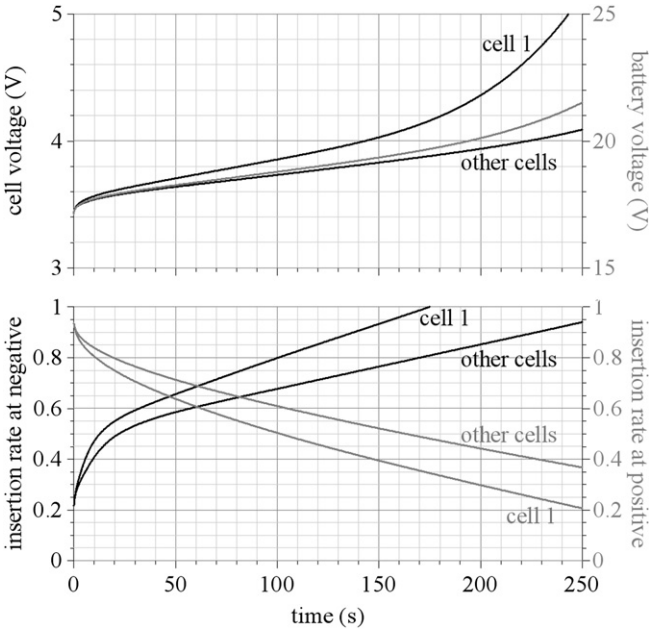

Fig. 12. Simulation of a 10C complete charge of a 5-cell battery (initial SOC: 100%, solid phase diffusion coefficients of cell 1: $D_{s,neg} = (2 \times 10^{-16})/2\ m^2\ s^{-1}$, $D_{s,pos} = (3.7 \times 10^{-16})/2\ m^2\ s^{-1}$.

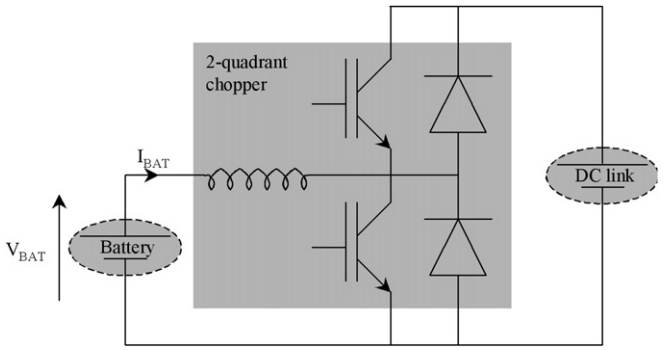

Fig. 13. Sketch of a power electronic structure associating a 14-cell lithium-ion battery and a two-quadrant chopper.

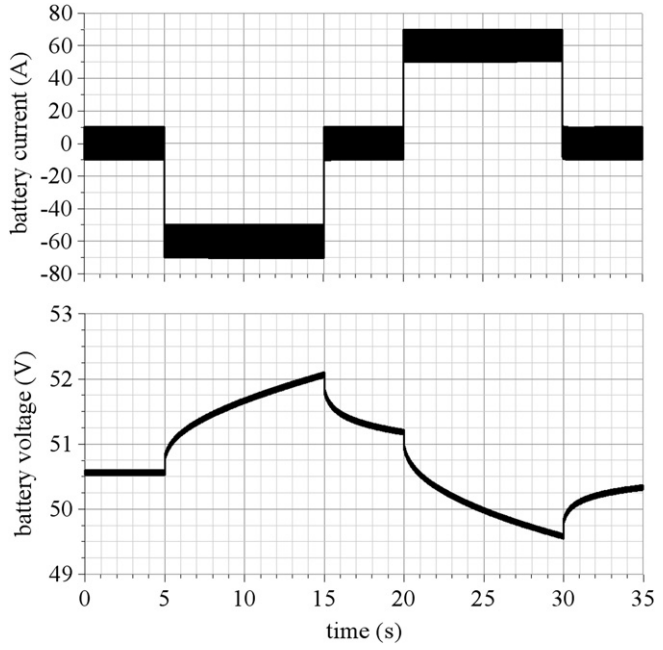

Fig. 14. Simulation of an association 14-cell lithium-ion battery/power electronic converter (initial SOC: 46%, temperature: 300 K, DC link voltage: 240 V, switching frequency: 2 kHz).

6. Conclusion

In this article, we detail a lithium-ion battery electrical model that includes transient description, double-layer phenomenon, and 1D mathematical representation of charge and mass transport phenomena in electrodes and electrolyte. For this purpose, electrical analogies of migration and diffusion are used, so that the model is directly implemented in simulation software dedicated to electrical circuit and electrical systems design. A comparison with results obtained by means of a finite element resolution method have shown that the use of electrical analogy for charge and mass transport representation gives nearly equivalent results. At last, a series operation and an association with a power electronic converter are simulated in order to show advantages of our modeling method for system oriented simulation. Of course, one of the main limit of this method is multi-dimension modeling: electrical analogy is suitable for 1D modeling, but not really for 2D or 3D modeling.

Further work has to be led to complete the model with an actual experimental characterization procedure, in order to identify model parameters. The model has also to be studied versus temperature, and coupled with a thermal model (based on electrical analogy) of the battery, in order to describe thermal runaway or electrothermal coupling phenomenon that may arise under some operating conditions, especially at low temperature (less than 0 °C).

References

[1] K. Smith, C.-Y. Wang, Journal of Power Sources 161 (no. 1) (October 2006) 628–639.
[2] M. Doyle, T.F. Fuller, J. Newman, Journal of the Electrochemical Society 140 (no. 6) (June 1993) 1526–1533.
[3] T.F. Fuller, M. Doyle, J. Newman, Journal of the Electrochemical Society 141 (1) (January 1994) 1–10.
[4] K. Smith, C.-Y. Wang, Journal of Power Sources 160 (1) (September 2006) 662–673.
[5] L. Cai, R.E. White, Journal of Power Sources 196 (14) (July 2011) 5985–5989.
[6] J.R. Macdonald, Impedance Spectroscopy – Emphasing Solid Materials and System, John Wiley and Sons Editions, 1987.
[7] T.A. Jossen, Journal of Power Sources 154 (2) (March 2006) 530–538.
[8] H.L. Chan, A new battery model for use with battery energy storage systems and electric vehicles power systems, In: Presented at IEEE Power Engineering Society Winter Meeting, vol. 1 (January 2000). Singapore, pp. 470–475.
[9] Y.H. Kim, H.D. Ha, IEEE Transactions on Industrial Electronics 44 (1) (February 1997) 81–86.
[10] I. Papic, IEEE Transactions on Energy Conversion 21 (2) (June 2006) 608–615.
[11] O. Tremblay, L.-A. Dessaint, A.-I. Dekkiche, A generic battery model for the dynamic simulation of hybrid electric vehicles, in: Presented at IEEE-VPPC 2007 (September 2007), pp. 284–289. Arlington.
[12] K. Kurohane, A. Uehara, T. Senjyu, A. Yona, N. Urasaki, T. Funabashi, C.-H. Kim, Renewable Energy 36 (1) (January 2011) 42–49.
[13] K. Bandara, T. Sweet, J. Ekanayake, Renewable Energy 37 (1) (January 2012) 82–88.
[14] A. Tofighi, M. Kalantar, Renewable Energy 36 (9) (September 2011) 2440–2450.
[15] M. Urbain, M. Hinaje, S. Raël, B. Davat, P. Desprez, IEEE Transactions on Energy Conversion 25 (3) (September 2010) 862–872.
[16] P. Mauracher, E. Karden, Journal of Power Sources 67 (1–2) (July–August 1997) 69–84.
[17] S. Buller, M. Thele, E. Karden, R.W. De Doncker, Journal of Power Sources 113 (2) (January 2003) 422–430.
[18] E. Kuhn, C. Forgez, P. Lagonotte, G. Friedrich, Journal of Power Sources 158 (2) (August 2006) 1490–1497.
[19] S. Buller, M. Thele, R.W. De Doncker, E. Karden, Impedance-based simulation models of supercapacitors and Li-ion batteries for power electronic applications, In: Presented IEEE-IAS 2003, vol. 3 (October 2003). Salt Lake City, pp. 1596–1600.
[20] A.M. Dhirde, N.V. Dale, H. Salehfar, M.D. Mann, T.H. Han, IEEE Transactions on Energy Conversion 25 (3) (September 2010) 778–786.
[21] K.A. Smith, C.D. Rahn, C.-Y. Wang, Energy Conversion and Management 48 (9) (September 2007) 2565–2578.
[22] G.-A. Nazri, G. Pistoia, Lithium Batteries: Science and Technology, Kluwer Academic Publishers, Boston, 2004.
[23] R.B. Bird, W.E. Stewaert, E.N. Lightfoot, Transport Phenomena, second ed., Wiley, New York, 2002.

Nomenclature

Latin letters
a: active surface per volume unit [m^{-1}]
A: active surface [m^2]
c: concentration [mol m^{-3}]
C_{DL}: electric double layer capacitor [F]
D: diffusion coefficient of species [m^2 s^{-1}]
F: Faraday's constant, 96,485 [C.mol^{-1}]
G^{Li}: volume rate of Li^+ generation [mol m^{-3} s^{-1}]
j_0: exchange current density [A m^{-2}]
j^{Li}: volume rate of Li^+ current generation [A m^{-3}]
J: current density [A m^{-2}]
I: current [A]
N: charge or species molar flow [mol s^{-1}]
p: Bruggeman exponent [–]
r: radial coordinate [m]
R: radius [m]
t: time [s]
t_p: Li^+ transference number [–]
T: temperature [K]

U: electrode equilibrium potential [V]
u_T: thermal voltage [V]
V: voltage [V]
x: Cartesian coordinate [m]

Greek letters
α: transfer coefficient [−]
δ: layer thickness [m]
ε: volume fraction [−]
η: surface overvoltage [V]
σ: electrical conductivity [S m^{-1}]
φ: charge or species molar flow density [mol m^{-2} s^{-1}]
ϕ: electrical potential [V]

Superscripts and subscripts
cell: battery cell
e: electrolyte phase
eff: effective value
init: initial value
mean: average value
neg: negative electrode
o: oxydation
pos: positive electrode
r: reduction
s: solid phase
s,e: solid/electrolyte interface
sep: separator